a beam in a biased crystal with $\Delta n_0 = 6 \times 10^{-4}$ and with a ratio between the peak intensity and the saturation intensity, $I(0)/I_{sat} = 3$, patterns form in several regions on the beam (Fig. 3). At the flat top of the beam, low visibility stripes appear. In this region, the nonlinearity is above threshold but in rather deep saturation, so the MI growth rate is suppressed. Then, at the margins of the beam, where the local ratio $I(r) + I_{sat}$ is around and slightly below unity, high-visibility stripes appear. In this region, the nonlinearity is above threshold and is not saturated, so the MI growth rate is large. Lastly, at the far margins of the beam, the local nonlinearity is below threshold, because $I(r) \ll I_{sat}$. A by-product of this particular experiment is the clear evidence (Fig. 3) that the 1D stripes emerge at different orientations and are not affected much by the local noise (striations).

We would also like to relate our nonlinear optical system to other nonlinear systems of weakly correlated particles. Our prediction and experimental observation implies that in such systems patterns will form spontaneously, provided the nonlinearity is larger than a threshold value, which in turn is set by the correlation distance. For example, we expect that 1D and 2D patterns will form in an atomic gas at temperatures slightly above the Bose-Einstein condensation temperature (at which the atoms possess independent degrees of freedom, yet are still weakly correlated). At least for atoms with attractive collision forces, whether natural [e.g., ^{7}Li (*23*)] or through magnetic tuning of the condensate self-interaction (*24*), such patterns should form. The equation governing the evolution of the "mean field" of an atomic gas is the Gross-Pitaevski equation (*25*), which almost fully coincides with the nonlinear wave equation that gives rise to (1+1)D Kerr solitons. The relevance of this work to cooled atomic gases is therefore obvious. In other areas of physics there are, in fact, at least some hints that such patterns do exist in disordered many-body nonlinear systems. To be specific, several experimental papers have reported a large anisotropy in the resistivity of a 2D electron system with weak disorder (*26*). The observed anisotropy is now attributed to the combination of nonlinear transport and weak disorder (*27*, *28*), which is the transport equivalent of nonlinearity and incoherence in optical systems such as ours. The theoretical works predict the existence of 1D stripes (electron stripes) of charge density wave. Spontaneous formation of stripes was also predicted and observed in high-T_c (superconducting transition temperature) superconductors (*29*), which is again a nonlinear weakly correlated many-body system. Lastly, as discussed in (*8*), spontaneously forming patterns are known in at least one system of classical particles: a gravitational system. The spontaneous emergence of patterns in all of these diverse fields of science indicates that pattern formation in nonlinear weakly correlated systems is a universal property. It is a gift of nature that in optics we can study directly, visualizing every little detail of the physics involved and isolating the underlying effects.

References and Notes

1. V. I. Bespalov and V. I. Talanov, *JETP Lett.* **3**, 307 (1966).
2. V. I. Karpman, *JETP Lett.* **6**, 277 (1967).
3. A. Hasegawa and W. F. Brinkman, *J. Quant. Electron.* **16**, 694 (1980).
4. For a review on MI in the temporal domain, see G. P. Agrawal, *Nonlinear Fiber Optics* (Academic Press, San Diego, CA, ed. 2, 1995), chap. 5 and references therein.
5. M. D. Iturbe-Castillo *et al.*, *Opt. Lett.* **20**, 1853 (1995).
6. M. I. Carvalho, S. R. Singh, D. N. Christodoulides, *Opt. Commun.* **126**, 167 (1996).
7. For a recent review on optical spatial solitons, see G. I. Stegeman and M. Segev, *Science* **286**, 1518 (1999).
8. M. Soljacic, M. Segev, T. H. Coskun, D. N. Christodoulides, A. Vishwanath, *Phys. Rev. Lett.* **84**, 467 (2000).
9. T. H. Coskun, D. N. Christodoulides, Y. Kim, Z. Chen, M. Soljacic, M. Segev, *Phys. Rev. Lett.* **84**, 2374 (2000).
10. M. Mitchell, Z. Chen, M. Shih, M. Segev, *Phys. Rev. Lett.* **77**, 490 (1996).
11. M. Mitchell and M. Segev, *Nature* **387**, 880 (1997).
12. D. N. Christodoulides T. H. Coskun, M. Mitchell, M. Segev, *Phys. Rev. Lett.* **78**, 646 (1997).
13. M. Mitchell, M. Segev, T. H. Coskun, D. N. Christodoulides, *Phys. Rev. Lett.* **79**, 4990 (1997).
14. A. W. Snyder and D. J. Mitchell, *Phys. Rev. Lett.* **80**, 1422 (1998).
15. V. V. Shkunov and D. Z. Anderson, *Phys. Rev. Lett.* **81**, 2683 (1998).
16. Z. Chen, M. Mitchell, M. Segev, T. H. Coskun, D. N. Christodoulides, *Science* **280**, 889 (1998).
17. D. N. Christodoulides, T. H. Coskun, M. Mitchell, Z. Chen, M. Segev, *Phys. Rev. Lett.* **80**, 5113 (1998).
18. N. Akhmediev, W. Krolikowski, A. W. Snyder, *Phys. Rev. Lett.* **81**, 4632 (1998).
19. O. Bang, D. Edmundson, W. Krolikowski, *Phys. Rev. Lett.* **83**, 4740 (1999).
20. M. Segev, G. C. Valley, B. Crosignani, P. DiPorto, A. Yariv, *Phys. Rev. Lett.* **73**, 3211 (1994).
21. D. N. Christodoulides and M. I. Carvalho, *J. Opt. Soc. Am. B* **12**, 1628, (1995).
22. M. Shih, M. Segev, G. C. Valley, G. Salamo, B. Crosignani, P. DiPorto, *Electron. Lett.* **31**, 826 (1995).
23. C. A. Sackett, J. M. Gerton, M. Welling, R. G. Hulet, *Phys. Rev. Lett.* **82**, 876 (1999).
24. S. L. Cornish, N. R. Claussen, J. L. Roberts, E. A. Cornell, C. E. Wieman, *Phys. Rev. Lett.* **85**, 1795 (2000).
25. Th. Busch and J. R. Anglin, *Phys. Rev. Lett.* **84**, 2298 (2000).
26. M. P. Lilly, K. B. Cooper, J. P. Eisenstein, L. N. Pfeiffer, K. W. West, *Phys. Rev. Lett.* **82**, 394 (1999); *Phys. Rev. Lett.* **83**, 824 (1999).
27. A. A. Koulakov, M. M. Fogler, B. I. Shklovskii, *Phys. Rev. Lett.* **76**, 499 (1996).
28. A. H. MacDonald and M. P. A. Fisher, *Phys. Rev. B* **61**, 5724 (2000).
29. V. J. Emery *et al.*, *Proc. Natl. Acad. Sci. U.S.A.* **96**, 8814 (1999), and references therein.

30. Supported by the Israeli Science Foundation, the National Science Foundation, the Army Research Office, the Air Force Office of Scientific Research, and the Deutsche Forschungsgemeinschaft. This work is part of the Multi University Research Initiative (MURI) project on optical spatial solitons.

2 June 2000; accepted 31 August 2000

Experimental Verification of Decoherence-Free Subspaces

Paul G. Kwiat,[1]* Andrew J. Berglund,[1]† Joseph B. Altepeter,[1] Andrew G. White[1,2]

Using spontaneous parametric down-conversion, we produce polarization-entangled states of two photons and characterize them using two-photon tomography to measure the density matrix. A controllable decoherence is imposed on the states by passing the photons through thick, adjustable birefringent elements. When the system is subject to collective decoherence, one particular entangled state is seen to be decoherence-free, as predicted by theory. Such decoherence-free systems may have an important role for the future of quantum computation and information processing.

Quantum computation holds the promise of greatly enhanced speeds for solving certain problems, including factoring (*1*), simulation of quantum systems (*2, 3*), and database searching (*4, 5*). One main obstacle to quantum computation is the problem of decoherence—fragile quantum superpositions are destroyed by unwanted coupling to the environment. In particular, it is the entangling of the quantum system to unobserved degrees of freedom that leads to a loss of coherence. (A related problem is that of dissipation, whereby energy is lost from the system.) Three basic strategies to cope with decoherence in quantum computation have emerged. The first, quantum error correcting codes, relies on trying to detect errors using ancillary quantum bits (qubits) and actively manipulating the interactions to correct these errors (*6, 7*). The second strategy employs dynamical decoupling, in which rapid switching is used to average out the effects of a relatively slowly decohering environment (*8*). The final approach attempts to embed the logical qubits

[1]Physics Division, P-23, Los Alamos National Laboratory, Los Alamos, NM 87545, USA. [2]Physics Department, University of Queensland, Brisbane, Queensland 4072, Australia.

*To whom correspondence should be addressed. E-mail: kwiat@lanl.gov

†Present address: Physics Department, California Institute of Technology, Pasadena, CA 91125, USA.

into a part of the overall Hilbert space that is inherently immune to noise, a "decoherence-free subspace" (DFS) (*9–16*) (typically, such a system is also "dissipation-free"). It has been shown that it should be possible to perform quantum computation operations without taking the system out of the DFS (*12, 13, 15*) and that the DFS is robust with respect to perturbations in the interactions (*12, 14*). Here, we present an experimental demonstration of the existence of a DFS, using entangled photons as our qubits.

The usual condition for a DFS is that the qubits under consideration are subject to collective decoherence—the disturbances affecting them are identical, as each individual qubit couples to the environment "bath" in the same way. When the system-environment interactions possess this sort of permutation symmetry, the decoherence-free states also display symmetry (e.g., are maximally entangled). This is a particular example of the more general requirement that some symmetry in the system-environment interaction decouples the DFS from the environment. Although not always applicable, this model of decoherence is nevertheless relevant for some implementations of quantum information processing, for instance, if the qubits are physically very close to each other and the environment cannot distinguish them.

Although formally one needs density matrices to describe a state after interaction with an environment, it is illustrative to view the action of the environment as adding a random phase shift $\langle\phi\rangle$ to each term in the state. For example, a decohering environment acting in the 0/1 basis will take $|0\rangle + |1\rangle \rightarrow e^{i\langle\phi_0\rangle}|0\rangle + e^{i\langle\phi_1\rangle}|1\rangle = e^{i\langle\phi_0\rangle}[|0\rangle + e^{i(\langle\phi_1\rangle - \langle\phi_0\rangle)}|1\rangle]$. The global phase is unobservable, but if the phases $\langle\phi_0\rangle$ and $\langle\phi_1\rangle$ are truly uncorrelated, then the qubit will be left in a mixed state; that is, the off-diagonal elements of the density matrix will vanish because of averaging over the random phases.

Consider two qubits in the "singlet" state $|\psi^-\rangle \equiv (|01\rangle - |10\rangle)/\sqrt{2}$. After coupling to the environment

$$\begin{aligned} |\psi^-\rangle \rightarrow\ & (e^{i\langle\phi_0\rangle}|0\rangle e^{i\langle\phi_1\rangle}|1\rangle \\ & - e^{i\langle\phi_1\rangle}|1\rangle e^{i\langle\phi_0\rangle}|0\rangle)/\sqrt{2} \\ = & e^{i(\langle\phi_0\rangle + \langle\phi_1\rangle)}(|01\rangle - |10\rangle)/\sqrt{2} \qquad (1) \end{aligned}$$

Because the global phase is unobservable, the initial state is preserved. One can now readily see why the decoherence needs to be collective: the phase will only factor out if the induced phases on qubit 1 are the same as those on qubit 2, as we implicitly assumed above.

The same argument predicts that the state $|\psi^+\rangle = (|01\rangle + |10\rangle)/\sqrt{2}$ is also decoherence-free. This is true if the environment acts only in the 0/1 basis (a "pure dephasing" environment) and, under this condition, the states $|\psi^\pm\rangle$ span a two-dimensional DFS, which may then be used as a logical qubit. However, an environment that acts in the diagonal basis, given by $|\pm\rangle \equiv (|0\rangle \pm |1\rangle)/\sqrt{2}$, causes "flipping" errors; a 0 can become a 1, and vice versa. Under this sort of collective decoherence, $|\psi^+\rangle$ is not decoherence-free, for $|\psi^+\rangle = (|++\rangle - |--\rangle)/\sqrt{2}$, which is completely decohered by the environment.

We can characterize the robustness of an arbitrary initial state ψ_{in} by calculating its overlap with the state after decoherence. This is the fidelity $F = \langle\psi_{in}|\rho_{out}|\psi_{in}\rangle$, where ρ_{out} is the final density matrix. If the input is not completely pure, as is typically the case for any experimentally produced state, we use the general definition $F = [\mathrm{Tr}(\sqrt{\rho_{in}}\rho_{out}\sqrt{\rho_{in}})^{1/2}]^2$ (*17*). For each of the four "Bell states" [$\psi^\pm \equiv (01 \pm 10)/\sqrt{2}$; $\phi^\pm \equiv (00 \pm 11)/\sqrt{2}$], the fidelity is plotted (Fig. 1) as a function of the basis angle θ of the collective decoherence (θ defines the two orthogonal linear polarization states between which the random phase shift is applied; for example, $\theta = 0°$ means decoherence in the 0/1 basis, $\theta = 45°$ means decoherence in the +/− basis, etc.). As expected, the singlet state ψ^- is always decoherence free (even in elliptical bases, because it always has the same antisymmetric form). In contrast, the state ϕ^+ decoheres in any (linear) basis, where it has the same form, $|\theta\theta\rangle + |\theta^\perp\theta^\perp\rangle$. The minimum fidelity resulting from this sort of collective decoherence is $F = 0.33$, for the states ϕ^- and ψ^+ at $\theta = 17.6°$ and 27.4°, respectively. This does not result simply because of a unitary transformation (e.g., a rotation) of the state; a plot of $\mathrm{Tr}(\rho_{out}^2)$ yields similar results, confirming that the dips truly arise from decoherence.

In order to have more than one state that is decoherence-free in all bases, one needs to have at least four entangled qubits (*11*) [though more recently it has been shown that three suffice to make a "noiseless subsystem" (*18*)]. However, for our proof-of-principle experiment, we restrict ourselves to the simplest system supporting a DFS: two qubits. Our qubits are represented by the polarization states ("0" ≡ H = horizontal; "1" ≡ V = vertical) of two correlated photons. The photon pairs are produced via the process of spontaneous parametric down-conversion in two thin, adjacent, nonlinear optical crystals [beta-barium-borate (BBO)] cut for type I phase matching (*19*). Inside the crystals, an ultraviolet pump photon (at 351 nm, produced from an 80-mW argon ion laser) may spontaneously split into two correlated daughter photons, emitted into different spatial modes. Because of energy conservation, the sum of the frequencies of these photons must equal that of the (monochromatic) parent photon; thus, the photons' frequencies are entangled.

Because of the details of the conversion process, an incident pump photon polarized at 45° will have equal probability amplitudes to down-convert in the first crystal, producing two H-polarized photons, or in the second crystal, producing two V-polarized photons. The coherence and high spatial overlap between these two processes lead to a very pure [~99% (*19*)] maximally entangled state $(|HH\rangle + |VV\rangle)/\sqrt{2}$. The other Bell states may be produced simply by exchanging H ↔ V in one arm and/or imposing a birefringent phase shift: H → H; V → − V.

The quantum mechanical state of the photons is characterized by tomographically measuring the density matrix or, more precisely, the two-photon contribution to the reduced density matrix corresponding to the polarization. This distinction will be important later. In essence, we determine the two-photon analogs of the usual Stokes parameters [see e.g., (*20*)] characterizing the polarization state of a single photon. We measure polarization correlations between the two photons for 16 analysis settings (e.g., HH, HV, 45°V, etc.), allowing reconstruction of the density matrix (*21*).

Experimentally, adjustable quarter- and half-wave plates and polarizing beam splitters in the two down-conversion beams allow polarization analysis in any basis (Fig. 2). The photons are detected by using silicon avalanche photodiodes operated in the geiger mode. Each detector is preceded by a small iris to define the spatial mode, a narrowband interference filter [centered at 702 nm, with a full width at half maximum of 5 nm (10 nm) in path 1 (path 2)] to reduce background and

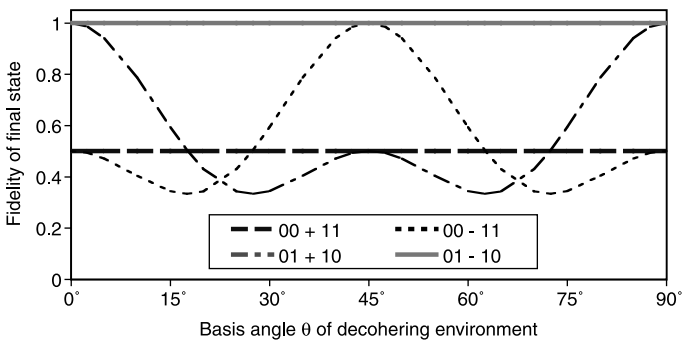

Fig. 1. Theoretically calculated fidelity of final state with initial Bell state, after collective decoherence in the (linear-polarization) basis $\theta/\theta^\perp$. The fidelity between any Bell state and a completely mixed state is 0.25; the minimum predicted fidelities are 0.33.

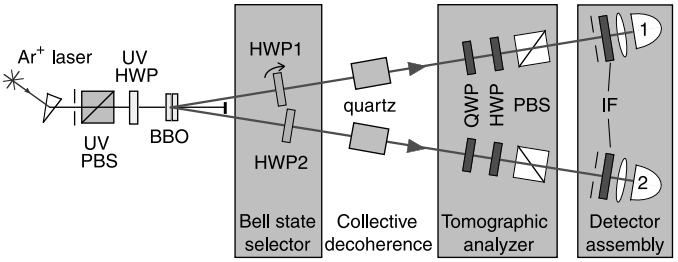

Fig. 2. Experimental arrangement used to investigate DFSs. Polarization-entangled photons are produced via spontaneous down-conversion in the adjacent nonlinear crystals (BBO). Half-waveplates (HWP1 and HWP2) are used to prepare the four Bell states. The decohering elements are ~10-mm samples of quartz; the element in path 1 is oriented at 17°, and the element in path 2 is at 17° + 90° = 107°, to permit collective decoherence in the presence of the intrinsic energy entanglement of the photons. The quartz separates the ordinary and extraordinary polarization components by more than the coherence length of the photons, determined by the interference filter (IF) before each detector. The final quarter-waveplate (QWP) and half-waveplate (HWP) in each arm, along with polarizing beam splitters (PBS), enable analysis of the polarization correlations in any basis, allowing tomographic reconstruction of the density matrix.

define the bandwidth of the photons, and a collection lens. The detector outputs are recorded in coincidence using a time-to-amplitude converter and a single-channel analyzer, leading to an effective coincidence window of ~5 ns; the resulting rate of accidental coincidences was less than 0.3 s^{-1}, compared to the typical rate of true coincidences, 30 s^{-1}.

The decoherence in our system is introduced as follows: In each arm, the photon passes through a ~10-mm-thick piece of quartz, with optic axis in the plane of the element. With this thickness, the ordinary and extraordinary polarization components are separated by $140\lambda_o$, where λ_o is the central wavelength of the photons (the plates were tilt adjusted so that the relative phase modulo 360° was zero). The coherence length of the photons (determined by the frequency filters and irises) is also $\sim 140\lambda_o$. Consequently, after passing through the quartz, the ordinary and extraordinary polarization components acquire a random relative phase. When we detect the photons, we essentially trace over the frequency degree of freedom, which plays the role of the "environment," and the resulting (reduced) density matrix for the polarization becomes mixed.

Actually, all decoherence is of precisely this sort: coupling to unobserved (and often unobservable) degrees of freedom. Although the total state, including both the quantum system of interest and the "environment" degrees of freedom, is in a pure state, the reduced density matrix of the quantum system alone (obtained by tracing over the environment) can be in a (partially) mixed state. Our quartz elements entangle the relative phase between the two production processes (in down-conversion crystal 1 or 2) with the photon's frequency. In the end, we trace over this degree of freedom; that is, we do not measure it, because our detectors are insensitive to wavelength (over the collection bandwidth). [The curves in Fig. 1 can be calculated by coupling the qubits' states to an imaginary measuring device and tracing over its final state or, alternatively, by using the total (polarization + frequency) state of the down-conversion photons, transformed by the quartz, and tracing over frequency (*22*). The resulting identical density matrices validate our technique for introducing decoherence.]

By setting the angles of the quartz elements appropriately, we can introduce "collective" decoherence in any desired (linear) basis. There is one subtlety: It is actually necessary to orient the pieces at 90° to each other, so that the decoherence effects are the same. By reversing the roles of the fast and slow axes in the quartz, one compensates for the frequency anticorrelations intrinsic to the down-conversion pairs (*22*). Otherwise, ϕ^+ appears to be the DFS.

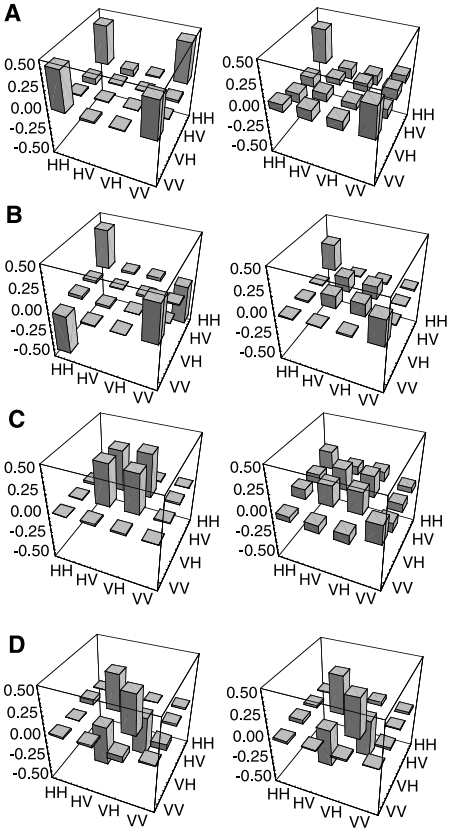

Fig. 3. Experimentally measured density matrices for the Bell states (**A**) HH + VV, (**B**) HH − VV, (**C**) HV + VH, and (**D**) HV − VH. The left panels represent the input states without decoherence; the right panels represent the resulting states after collective decoherence is applied in the 17° basis. Only the real parts are shown; the imaginary components, which theoretically are strictly zero, were always less than a few percent.

Table 1. Summary of DFS data for the four Bell states, before and after collective decoherence (in the 17° basis). The $F_{out-pure}$ and $F_{out-init}$ columns list the fidelity of the final state with the target Bell state and with the experimentally produced initial state, respectively; the F_{theory} column lists the theoretically expected value; and the $F_{out-theory}$ column lists the fidelity of the final state with the theoretical prediction.

Bell state	$F_{out-pure}$*	$F_{out-init}$*	F_{theory}†	$F_{out-theory}$*
HH + VV	0.51 ± 0.03	0.54 ± 0.04	0.5	1.00 ± 0.02
HH − VV	0.35 ± 0.02	0.34 ± 0.02	0.33 ± 0.01	0.98 ± 0.02
HV + VH	0.54 ± 0.02	0.53 ± 0.02	0.52 ± 0.02	0.99 ± 0.02
HV − VH	0.97 ± 0.04	1.00 ± 0.04	1	0.97 ± 0.04

*Uncertainties due to counting statistics. †Uncertainty due to a 0.5° uncertainty in the basis orientation θ of the decohering elements. From Fig. 1, we see that ψ^+ is most affected, whereas ϕ^+ and ψ^- are totally unaffected.

Figure 3 shows the measured density matrices for the Bell states. On the left are the states without decoherence, and on the right are the states after being decohered by quartz pieces at 17° (and 107°). The singlet state ψ^- is nearly perfectly preserved. This is made more quantitative by the measured fidelities, listed in Table 1. In all cases, there is excellent agreement between experiment and theory.

Our results demonstrate that we can experimentally and quantitatively study various aspects regarding error-free subspaces (of small quantum systems), with measurement accuracies at the percent level. For example, the effect of noncollective decoherence can be studied by changing the relative thickness and/or orientation of our "environments." The rate of decoherence can be very simply altered by changing the degree to which we trace out the environmental degrees of freedom, i.e., by adjusting the frequency bandwidth of the collection filters. Moreover, we expect that we can readily examine the case of larger

DFSs, either by looking at three- and four-photon events or, more easily, by using more degrees of freedom of the photon pairs (*23, 24*). For example, one might employ the entangled spatial modes to represent additional qubits while relying on frequency techniques to produce decoherence. Finally, we can extend our investigations to include dissipation by introducing controllable polarization-dependent losses.

References and Notes

1. P. W. Shor, in *Proceedings of the 35th Annual Symposium on Foundations of Computer Science*, S. Goldwasser, Ed. (IEEE Computer Society, Los Alamitos, CA, 1994), p. 116.
2. R. Feynman, *Int. J. Theor. Phys.* **21**, 467 (1982).
3. S. Somaroo, C. H. Tseng, T. F. Havel, R. Laflamme, D. G. Cory, *Phys. Rev. Lett.* **82**, 5381 (1999).
4. L. K. Grover, *Phys. Rev. Lett.* **79**, 325 (1997).
5. N. J. Cerf, L. K. Grover, C. P. Williams, *Phys. Rev. A* **61**, 32303 (2000).
6. D. Gottesman, *Phys. Rev. A* **54**, 1862 (1996).
7. C. H. Bennett, P. W. Shor, *IEEE Trans. Inf. Theory* **44**, 2724 (1998).
8. L. Viola, E. Knill, S. Lloyd, *Phys. Rev. Lett.* **82**, 2417 (1999).
9. G. M. Palma, K.-A. Suominen, A. K. Ekert, *Proc. R. Soc. London Ser. A* **452**, 567 (1996).
10. L.-M. Duan, G.-C. Guo, *Phys. Rev. Lett.* **79**, 1953 (1997).
11. P. Zanardi, M. Rasetti, *Phys. Rev. Lett.* **79**, 3306 (1997).
12. D. A. Lidar, I. L. Chuang, K. B. Whaley, *Phys. Rev. Lett.* **81**, 2594 (1998).
13. P. Zanardi, *Phys. Rev. A* **60**, R729 (1999).
14. D. Bacon, D. A. Lidar, K. B. Whaley, *Phys. Rev. A* **60**, 1944 (1999).
15. J. Kempe, D. Bacon, D. A. Lidar, K. B. Whaley, E-print available at http://xxx.lanl.gov/abs/quant-ph/0004064.
16. A. Beige, D. Braun, B. Tregenna, P. L. Knight, *Phys. Rev. Lett.* **85**, 1762 (2000).
17. R. Jozsa, *J. Mod. Opt.* **41**, 2315 (1994).
18. E. Knill, R. Laflamme, L. Viola, *Phys. Rev. Lett.* **84**, 2525 (2000).
19. P. G. Kwiat, E. Waks, A. G. White, I. Appelbaum, P. H. Eberhard, *Phys. Rev. A.* **60**, R773 (1999).
20. M. Born, E. Wolf, *Principles of Optics* (Cambridge Univ. Press, Cambridge, 1999).
21. A. G. White, D. F. V. James, P. H. Eberhard, P. G. Kwiat, *Phys. Rev. Lett.* **83**, 3103 (1999).
22. A. J. Berglund, thesis, Dartmouth College, Hanover, NH (2000) (E-print available at http://xxx.lanl.gov/abs/quant-ph/0010001).
23. P. G. Kwiat, *J. Mod. Opt.* **44**, 2173 (1997).
24. _____, J. R. Mitchell, P. D. D. Schwindt, A. G. White, *J. Mod. Opt.* **47**, 257 (2000).

25. We thank S. Barraza-Lopez and D. James for assistance and D. Lidar and L. Viola for valuable discussions. This work was supported in part by the National Security Agency and Advanced Research and Development Activity (ARDA) under contract MOD-713700.

13 June 2000; accepted 29 August 2000

Electronic Structure of Solids with Competing Periodic Potentials

J. Voit,[1]* L. Perfetti,[2] F. Zwick,[2] H. Berger,[2] G. Margaritondo,[2] G. Grüner,[3] H. Höchst,[4] M. Grioni[2]*

When electrons are subject to a potential with two incommensurate periods, translational invariance is lost, and no periodic band structure is expected. However, model calculations based on nearly free one-dimensional electrons and experimental results from high-resolution photoemission spectroscopy on a quasi–one-dimensional material do show dispersing band states with signatures of both periodicities. Apparent band structures are generated by the nonuniform distribution of electronic spectral weight over the complex eigenvalue spectrum.

One of the basic tenets of solid state physics is that the periodicity of the crystal lattice determines the electronic structure (*1*). The band structure of a crystalline solid differs from the free-electron dispersion $E(k) = \hbar^2k^2/2m$ (k, wave vector; $\hbar$, Planck's constant divided by 2π; m, electron mass) most fundamentally by the effects of Bragg reflection on the crystal lattice, which opens gaps at the Brillouin zone (BZ) boundaries and folds back dispersion branches into the first BZ (1BZ). The complete band structure can then be represented equivalently in the reduced, extended, or repeated zone schemes. By contrast, genuine aperiodic (glassy or amorphous) systems would not show dispersing bands.

Important questions for the understanding of band structures are, What are the states of electrons in quasiperiodic systems, or in a potential with two competing, incommensurate periodicities? Are they still periodic? What would experimental probes of "band structures," such as angle-resolved photoemission spectroscopy (ARPES), observe? If the two periodicities Q_1 and Q_2 are commensurate (Q_1/Q_2 is a rational number) or can be reduced to a commensurate approximant, one can recover a consistent description of the electronic structure in the reduced 1BZ of the longer periodicity, although even here, the relevance of this reduced zone for experiments is unclear. More delicate is the case where the two potentials are truly incommensurate (Q_1/Q_2 is an irrational number). Typical examples are quasi–one-dimensional Peierls systems where, below a critical temperature T_P, a lattice modulation and an electronic charge-density wave (CDW) with twice the Fermi wave number ($2k_F$, unrelated to the lattice periodicity) form because of electron-phonon coupling (*2*).

With two incommensurate periods, translational invariance is lost, and the electronic states can no longer be classified according to wave numbers k. One expects a hierarchy of energy levels whose distribution will depend, among other factors, on the periods of the potential. Such level schemes have been calculated for a few theoretical problems, the most famous being the Hofstadter butterfly spectrum of two-dimensional electrons in a magnetic field (*3*). Other examples include one-dimensional (1D) quasicrystals (*4*) or soliton states in 1D Peierls models (*5*). However, it is not clear that such complex nondispersive level structures can be observed directly. X-ray diffraction of incommensurate structures still gives sharp peaks, so that the two underlying periodicities are correctly "recognized." The two problems, however, are not equivalent. The x-ray pattern is the Fourier transform of the electronic density distribution, whereas no similar relation exists for the electronic structure.

Using a simple model of 1D electrons in incommensurate potentials, we show that, despite the collapse of the BZ, the spectral weight of photoelectrons is peaked at "bands" close to the free-electron parabola. In an extended zone scheme, these bands are modulated by the strength of the potentials and exhibit gaps at the appropriate wave vectors. We find similar structures in high-resolution ARPES experiments on a typical 1D Peierls material, $(TaSe_4)_2I$. We observe, however, additional subtleties, which we explain with a model specific to $(TaSe_4)_2I$.

First, we consider 1D tight-binding electrons (lattice constant a; $Q_1 = 2\pi/a$) in a superstructure with a commensurate period $4a$ ($Q_2 = \pi/2a$). Such a superstructure could arise from a Peierls transition in a quarter-filled conduction band. The Hamiltonian is

[1]Theoretische Physik 1, Universität Bayreuth, D-95440 Bayreuth, Germany. [2]Institut de Physique Appliquée, Ecole Polytechnique Fédérale, CH-1015 Lausanne, Switzerland. [3]Department of Physics, University of California, Los Angeles, CA 90095–1547, USA. [4]Synchrotron Radiation Center, University of Wisconsin–Madison, Stoughton, WI 53589–3097, USA.

*To whom correspondence should be addressed. E-mail: johannes.voit@uni-bayreuth.de (J.V.) and marco.grioni@epfl.ch (M.G.)